# Abnormal Raman Intensity of Single-Walled Carbon Nanotubes Grown on Silica Spheres

**Jinyong Wang, Rongli Cui, Yu Liu, Weiwei Zhou, Zhong Jin, and Yan Li\***

*Beijing National Laboratory for Molecular Sciences, National Laboratory of Rare Earth Material Chemistry and Application, Key Laboratory for the Physics and Chemistry of Nanodevices, College of Chemistry and Molecular Engineering, Peking University, Beijing 100871, China*

Resonant Raman scattering experiments are carried on single-walled carbon nanotubes (SWCNTs) suspended between silica spheres. Weak uniaxial strain is introduced into these tubes during the chemical vapor deposition growth process. The metallic nanotubes exhibit different behavior from their semiconducting counterparts under the uniaxial strain. The G band shows no change in position and shape for metallic nanotubes, while for semiconducting nanotubes the G mode changes in profile but does not change in position. The radial breathing mode (RBM) maintains its position under the uniaxial strain for all the tubes. Most of the Raman spectra show an intense RBM, even for large diameter (∼2 nm) semiconducting SWCNTs and armchair SWCNTs. The large RBM/G band intensity ratio is ascribed to the much longer lifetime of the excited electronic states in the resonant process.

## 1. Introduction

Single-walled carbon nanotubes (SWCNTs) have attracted much attention because of their unique structures and remarkable electrical and optical properties.[1] Spectroscopy, especially resonant Raman spectroscopy, has provided a powerful and nondestructive tool for the characterization of SWCNTs.[2-6]

Resonant Raman spectroscopy has been widely used in the study of both bulk SWCNTs and isolated SWCNTs.[3-5,7-9] The radial breathing mode (RBM) at low frequency (normally $100-400$ cm$^{-1}$) and the high-frequency tangential mode (G band) around 1590 cm$^{-1}$ are the two important Raman active features of SWCNTs.[4] From the Raman active feature position and intensity, the electronic, vibrational, and structural properties can be derived. The RBM frequency has been proven to be dependent on the diameter $d_t$ through the relation $\omega_{RBM} = a/d_t + b$ by theoretical calculation and experimental data, where $a$ and $b$ are empirically derived parameters.[5,10-12] $a = 248$ cm$^{-1}$ nm and $b = 0$ has been found for isolated SWCNTs on an oxidized Si substrate (using a C–C bond distance of 0.144 nm).[5] $a = 223.5$ cm$^{-1}$ and $b = 12.5$ cm$^{-1}$ (using a C–C bond distance of 0.144 nm) was determined from Raman measurements for HiPco tubes in surfactant suspensions.[13] For suspended isolated SWCNTs, $a = 204$ cm$^{-1}$ nm and $b = 27$ cm$^{-1}$ (using a C–C bond distance of 0.142 nm) was derived by electron diffraction and Raman study and has been proven to give a good relation between $\omega_{RBM}$ and $d_t$ by many groups through Rayleigh scattering and Raman spectra.[14-16] The $(n, m)$ indices of SWCNTs can be determined by its diameter and transition energy using the so-called Kataura plot.[17]

The intensity of the Raman modes varies for SWCNTs with different diameters and chiral angles.[18-21] There are many factors that determine the Raman intensity, such as the laser energy, the electron–phonon coupling matrix element, and the electron–photon dipole matrix element. Raman intensity is proportional to the square of the electron–phonon coupling matrix element.[4,22,23] The electron–phonon matrix element has been calculated by

many groups.[20,24,25] The value of the matrix element depends on nanotube diameter, chiral angle, and the particular optical transition. It is found by theoretical study that the matrix element of the RBM decreases significantly with an increase in nanotube diameter and chiral angle, while the matrix element of G band is less sensitive to $(n, m)$ indices.[20,24] For SWCNTs with relatively large diameter and chiral angle, the RBM intensity is weak. It was found by ab initio calculations that the strength of the electron–phonon coupling matrix element of high-energy modes is up to 6 times higher than for that of the RBM.[25] Because of the larger phonon energy of G band than that of the RBM, the G band always has a much broader resonance window than the RBM. Thus, in most cases the G band is much stronger than the RBM.

Many factors show influence on the Raman frequency and intensity, for example the surrounding environment, the charge transfer, the strain, the temperature, and the interactions between SWCNTs and other species.[26-29] Among these factors, the effect of strain on SWCNTs is still not very clear. Many controversial results exist. In most of the previous studies on uniaxial strain deformation upon the Raman, SWCNTs deposited on a silicon substrate were usually used, and a force perpendicular to the nanotube axis was applied to introduce the uniaxial strain by the AFM tip.[30-32] Torsional deformation and substrate effect might be also introduced into the nanotube at the same time, which makes the results contradictory. Recently, more reliable Raman measurements of SWCNTs under strain were carried on individual suspended SWCNTs.[33] However only semiconducting SWCNTs were examined. In order to fully understand the uniaxial strain effect on Raman spectra, further study on metallic SWCNTs should be performed.

In the present work, resonant Raman spectra are performed on SWCNTs suspended between submicron silica spheres. A large variation in the nanotube RBM intensity is observed for both semiconducting and metallic nanotubes. Among the 136 detected nanotubes, 103 of them have an intensity larger for the RBM than for the G band. It is found that uniaxial strain is introduced into the suspended SWCNTs between silica spheres, which causes an abnormally strong RBM band. The uniaxial

* To whom correspondence should be addressed. Phone/fax: +86-10-62756773. E-mail: yanli@pku.edu.cn.
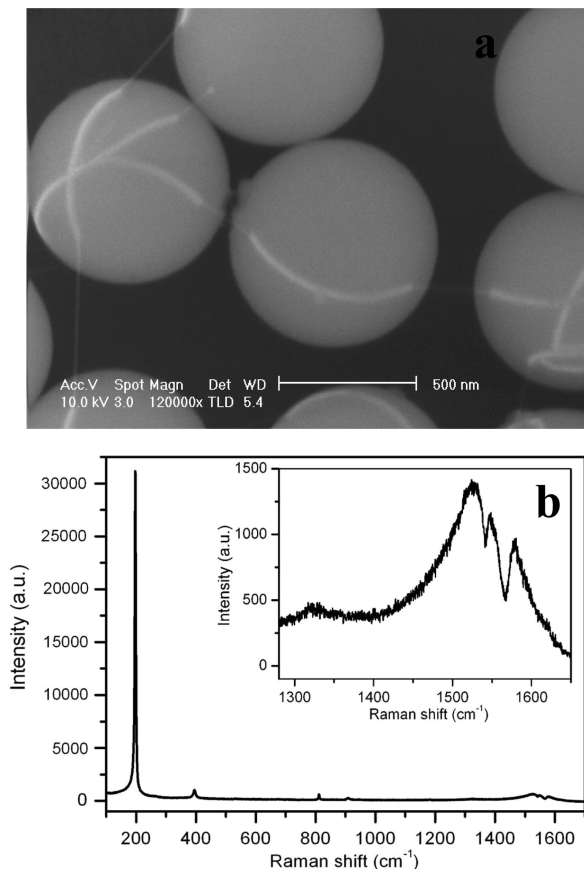
**5076**  *J. Phys. Chem. C, Vol. 113, No. 13, 2009*

Wang et al.

**Figure 1.** (a) SEM image of SWCNTs grown on 700 nm silica spheres. (b) Typical Raman spectrum with an intense RBM for SWCNT on silica spheres. The inset is the magnified G band part.

**TABLE 1: Observed and Predicted RBM Frequencies, Electronic Transition Energy, and Assignment for Metallic SWCNTs with an Intense RBM**

| $(n, m)$ | diameter $d_t$ (nm) | experimental $\omega_{RBM}$ (cm$^{-1}$) | calculated $\omega_{RBM}$ (cm$^{-1}$) | $E_{11}^L$ | $E_{11}^R$ |
|---|---|---|---|---|---|
| (13, 4) | 1.205 | 195, 196, 197 | 196 | 1.852 | 1.984 |
| (12, 6) | 1.243 | 190, 191 | 191 | 1.833 | 1.910 |
| (9, 9) | 1.220 | 193, 194 | 194 | 1.918 | 1.918 |
| (14, 2) | 1.182 | 198, 199 | 200 | 1.861 | 2.039 |
| (15, 3) | 1.308 | 184 | 183 | 1.727 | 1.862 |
| unresolved | | 185, 186, 187 | | | |
| (16, 1) and | 1.294 | | 185 | 1.733 | 1.891 |
| (11, 8) | | | | | |
| | 1.294 | | 185 | 1.801 | 1.831 |

Supporting Information. The Raman spectra with high intensity come from the suspended SWCNTs. In this sense, our data are free of environmental effects.

In a typical Raman experiment of SWCNTs, the RBM is normally more difficult to detect and much weaker than the G band. However, in the present study, for the suspended nanotubes between silica spheres, many of the Raman signals have an intensity larger for the RBM than for the G band. Actually, among the 136 detected nanotubes, 103 of them have a intensity larger for the RBM than for the G band. Figure 1b shows a typical Raman spectrum with a high RBM/G band intensity ratio. The G band is almost invisible compared to the RBM. For an individual SWCNT, its Raman spectrum can be detected only when electron transition energy matches the laser energy. The resonant Raman window of the RBM for isolated SWCNTs is around a few tens of meV; thus, the RBM peaks can be detected only when electron transition energy is very close to the laser energy. It is reasonable to assume that for each tube detected with strong intensity of the RBM, the electron transition energy is very close to the laser energy. The trigonal warping effect causes a tube-chirality-dependent splitting of each van Hove singularity for metallic nanotubes into lower ($E_{ii}^L$) and higher ($E_{ii}^R$) energy components. The Raman spectra is usually too weak to be detected when resonance with $E_{ii}^R$ because of the smaller magnitude of the matrix element along K-Γ than that in the K-M direction.[38] For metallic SWCNTs, the RBM peaks can be detected only when the $E_{ii}^L$ is very close to the laser energy. Table 1 is a summary of the assignment for suspended metallic SWCNTs on silica spheres with a strong RBM/G band intensity ratio. The diameter is determined using the expression given by Meyer et al., $\omega_{RBM} = 204$ cm$^{-1}/d_t + 27$ cm$^{-1}$, which was widely used in a previous study on suspended SWCNTs.[14] The transition energy is determined by the verified results in Raman experiment by Strano.[39]

From Table 1, it can be seen that the $E_{ii}^L$ of these metallic SWCNTs deviates from 1.96 eV significantly, except for the (9, 9) nanotubes. The RBM should not have been observed, as the $E_{ii}^L$ of the nanotube moves out of the resonance region; thus, there must be a shift of the transition energy (may be none for the (9, 9) nanotubes). In our case, the SWCNTs are free of substrate influence. From the SEM image in Figure 1a, it can be seen that there is no obvious deformation perpendicular to the tube axis for the suspended SWCNTs. Therefore, uniaxial strain should be the most probable factor that shifts the transition energy. According to previous theoretical and experimental studies, the band structure of the SWCNTs changes as strain is applied in the uniaxial direction except for the armchair nanotubes.[40,41] For all metallic SWCNTs excluding the armchair nanotubes, the lower energy component $E_{11}^L$ increases proportionally to the uniaxial strain following an $n - m =$ constant

strain effect on the metallic and semiconducting SWCNTs is also examined.

## 2. Experimental Section

Isolated SWCNTs on silica spheres were grown using our published chemical vapor deposition (CVD) method.[34] The partially suspended SWCNTs on a trench-contained silicon wafer were grown using our ultralow feeding gas flow CVD method.[35] Raman spectra were collected on a Jobin Yvon LabRam HR 800 micro-Raman spectrometer with an excitation wavelength of 632.8 nm. A 100× air objective was used, and the spot size was about 1 $\mu$m$^2$. The laser energy was controlled at about 1 mW to avoid any heat effect.

## 3. Results and Discussion

Figure 1a shows a typical SEM image of SWCNTs on silica spheres. The diameter of the silica spheres is ~700 nm. It can be seen that there are two different kinds of SWCNTs on the silica sphere: SWCNTs suspended between the neighboring silica spheres and SWCNTs adhered to the surface of silica spheres. It was found by many groups that Raman spectra of suspended SWCNT has a higher intensity than the same SWCNT on the substrate due to the substrate-induced nonradiative decay of excitons in SWCNT.[15,33,36,37] In our Raman experiment, a relatively short acquisition time (≤30 s) is used and the Raman spectra with weak intensity (≤2000 counts for the strongest peak when the acquisition time is 30 s) is abandoned. Thus SWCNTs suspended between silica spheres could be distinguished from SWCNTs on silica surface by their Raman intensity. A more detailed description is available in
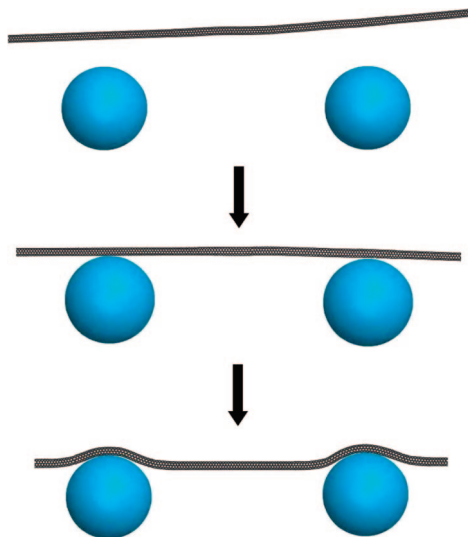
Single-Walled Carbon Nanotubes Grown on Silica

*J. Phys. Chem. C, Vol. 113, No. 13, 2009* **5077**

**SCHEME 1: Schematic Representation of the Interactions between SWCNTs and Silica Spheres**[a]



[a] (i) The nanotube grows in a floating manner. (ii) When suffering from some perturbation, the floating nanotube adheres to the surface of the two neighboring silica spheres. (iii) Because of the strong interaction between SWCNTs and SiO₂, a curved superstructure is formed. Thus, a strong uniaxial strain is introduced into the SWCNT.

pattern, while the higher energy component $E_{11}^R$ decreases under the uniaxial strain.[42] The predicted results are in good accordance with the experimental data as shown in Table 1. It must be emphasized that uniaxial strain does not shift the frequency of the RBM; thus, our assignment results are reliable. For metallic SWCNTs whose interband transition energy is above 1.96 eV, their transition energy $E_{11}^L$ gets larger and deviates from their resonance window; thus, these nanotubes cannot be observed in our experiment. The assignment of semiconducting SWCNTs with an intense RBM is called into question. When using the 1.96 eV laser, the diameter of the semiconducting SWCNTs detected is relatively large, and the precise transition energy of the nanotubes is needed to distinguish the semiconducting SWCNTs with similar diameters. It is hard for us to determine how much the transition energy has shifted; thus, no systemic assignment is performed on the semiconducting SWCNTs.

The uniaxial strain is introduced into the carbon nanotubes from several sources. In a typical growth experiment, CVD is preceded at 900 °C. When the sample cooled to the room temperature, the suspended SWCNTs between two silica spheres could be contracted by about 1‰.[43] The interaction between silica spheres and SWCNTs also plays an important role. Because the SWCNTs could grow across the space between two neighboring silica spheres, the nanotubes should grow in a floating manner.[44] When suffering from some perturbation, the floating nanotube adhered to the surface of two neighboring silica spheres. Because the interactions between SWCNTs and SiO₂ can be as large as 2−3 eV/nm,[45,46] a curved superstructure should be formed. Then the suspended SWCNTs should suffer an additional force along the uniaxial direction (Scheme 1). The gas flow may also introduce uniaxial strain into our nanotube in the CVD growth process. Our analysis based on SEM images and theoretical discussion in Supporting Information provides more evidence to back up the existence of the strain.

In our sample, the strain on the tubes is not uniform for the SWCNTs at different regions. Thus, it provides us a possibility to study the uniaxial strain effect on the SWCNTs. The Raman spectra of metallic SWCNTs exhibit different behavior from
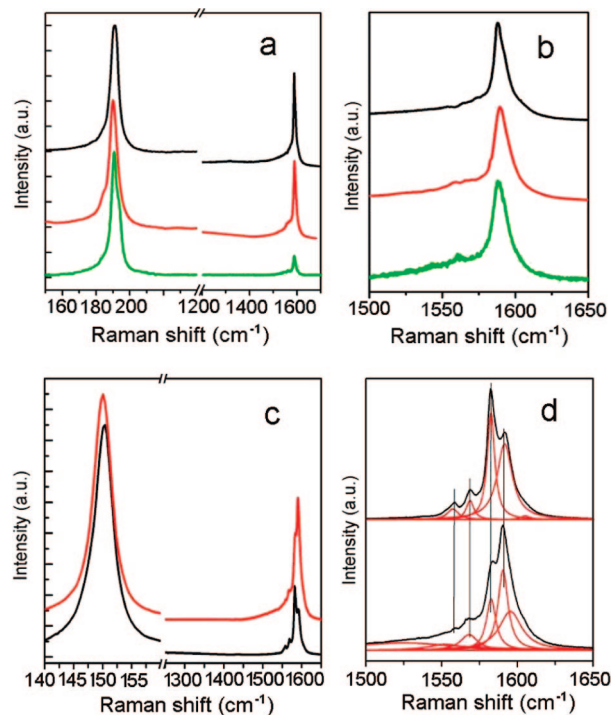


**Figure 2.** (a and c) Raman spectra for metallic (12, 6) and semiconducting (16, 8) SWCNTs, respectively; (b and d) the corresponding G band parts.

that of the semiconducting SWCNTs. Figure 2 shows Raman spectra of (12, 6) (metallic) and (16, 8) (semiconducting) SWCNTs, respectively. The spectra have been normalized with respect to the intensity of the RBM. Figure 2b,d shows their G band parts. In order to make the relationship among the spectra readily apparent, the spectra in Figure 2b,d are scaled. The RBM frequency does not show obvious shift for both metallic and semiconducting SWCNTs, which indicates that the RBM frequency is not sensitive to the uniaxial strain, which is in agreement with previous experimental results.[33] The uniaxial strain induces no increase in defects, as no obvious D peaks are visible. The intensity ratio of RBM/G is sensitive to the value of the strain. The electronic transition energy is verified with the change in uniaxial strain. Because of its small resonance window, the RBM intensity changes significantly as the nanotube moves into and out of resonance. Thus, the overall intensity ratio of the RBM/G mode changes dramatically with the change of the uniaxial strain. When the G mode is considered, significant differences are observed for different types of SWCNTs. The G mode of metallic SWCNTs does not change in an obvious way. However, for semiconducting SWCNTs, the G mode changes in profile but does not change significantly in position. This shows that the G mode of semiconducting nanotubes is more easily influenced than that of the metallic nanotubes under uniaxial strain.

For the RBM and G band, the resonant Raman scattering intensity for the Stokes process can be calculated by,

$$I(\omega, E_L) = C\left(\frac{E_a}{E_j}\right)[n(q,\mu) + 1]\sum_j$$
$$\left|\sum_a \frac{M^d(k-q,jb)M^{ep}(q,ba)M^d(k,aj)}{[E_L - (E_a - E_j) - i\gamma][E_L - (E_a - E_j) - h\omega - i\gamma]}\right|^2$$

where $C$ is a constant independent of $(n, m)$, $n(q, \mu)$ is the phonon thermal factor given by $n(q, \mu) = (e^{-E_{ph}/K_BT} - 1)^{-1}$ while j, a, and b denote the initial state, the excited states, and the
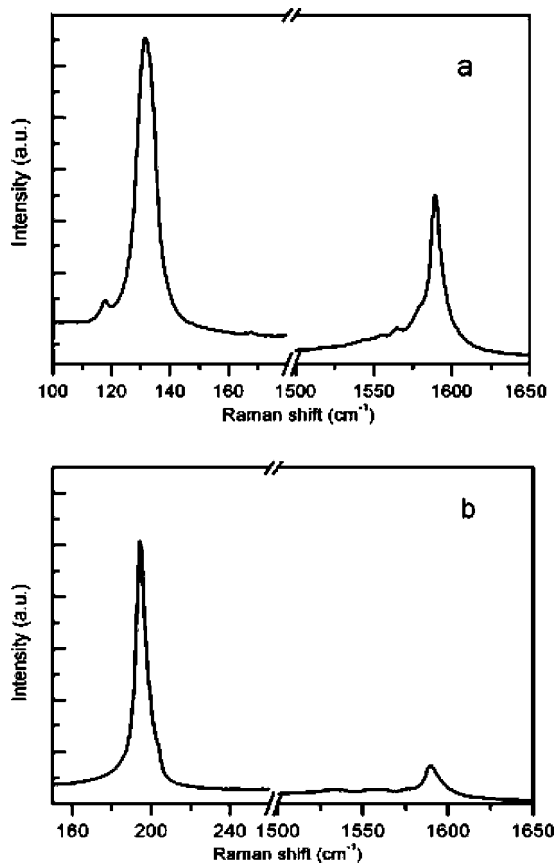
**5078** *J. Phys. Chem. C, Vol. 113, No. 13, 2009*

Wang et al.



**Figure 3.** Raman spectra for a large diameter SWCNTs (~1.946 nm) (a) and a (9, 9) armchair SWCNT (b) with a large RBM/G band intensity ratio.



**Figure 4.** The square of denominator ratio as a function of $\gamma$. The phonon energy is 0.2 eV and 0.02 eV, respectively, for the G mode and the RBM. $R^{1/2} = (E_L - E_a + E_j - i\gamma)(E_L - E_a + E_j - h\omega_{RBM} - i\gamma)/[(E_L - E_a + E_j - i\gamma) (E_L - E_a + E_j - h\omega_{RBM} - i\gamma)]$.

scattered state of an electron, respectively. $E_L$, $E_a$, and $E_j$ are the energies of the laser, the initial state, and the excited states, respectively. $\gamma$ is the broadening factor, which is determined by the inverse lifetime of the carriers in the resonant process. As can be seen from the equation, there are a few factors which show influence on the intensity of the RBM and G band: the difference between laser energy and the electron transition energy, the dipole matrix elements of the electron−photon interaction $M^d$, electron−phonon interaction matrix elements $M^{ep}$, the phonon thermal factor $n(q, \mu)$, and the broadening factor $\gamma$.

In our case, the laser energy is low enough to avoid any heat effect, thus the phonon thermal factor $n(q, \mu)$ is a constant for the RBM and G band. When the intensity ratio of the RBM and G band is considered, the dipole matrix elements of the electron-photon interaction $M^d$ can be neglected. The strong RBM intensity enhancement can be understood in terms of energy difference denominators and electron−phonon coupling strength in the above equation.

According to previous study, the strength of the electron−phonon coupling matrix element of G modes is higher than that of the RBM.[25] The matrix element of the RBM decreases significantly with an increase in the nanotube diameter and chiral angle. For nanotubes with a large diameter and chiral angle, the RBM should be weak. However, in the present study, large diameter SWCNTs (~1.946 nm, for the nanotube in Figure 3a) and (9, 9) armchair SWCNTs (Figure 3b) are found with a large RBM/G band intensity ratio, too. The electron−phonon coupling matrix element has the form of an inner product of the amplitude and eigenvector of the phonon, and deformation potential vector. The deformation potential is given by gradient of the crystal
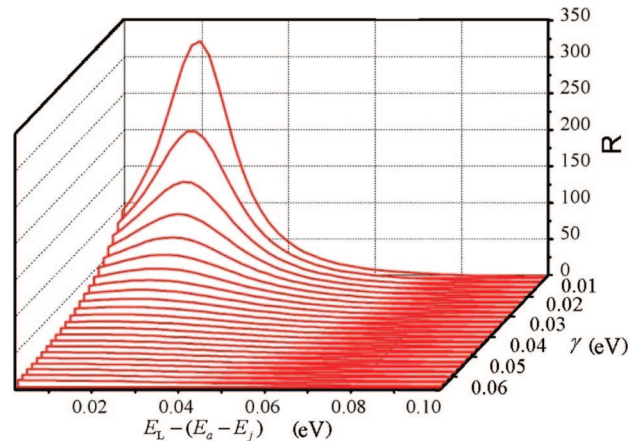
potential. In our study, since the uniaxial strain is not very large, the frequency of the RBM and G band shows no obvious shift, and the deformation potential, the amplitude and eigenvector of the phonon remains almost unchanged. The value of electron−phonon coupling matrix element is nearly a constant. Therefore, the large RBM/G band intensity ratio reflects that the denominator in the above equation can be much smaller in the case of the RBM than in the case of the G mode.

In Figure 4 we calculate the square of the denominator ratio $(E_L - E_a + E_j - i\gamma) (E_L - E_a + E_j - h\omega_G - i\gamma)/ [(E_L - E_a + E_j - i\gamma) (E_L - E_a + E_j - h\omega_{RBM} - i\gamma)]$ as the function of $\gamma$, at the phonon energy 0.2 eV and 0.02 eV, respectively, for the G mode and the RBM. The RBM/G intensity ratio is proportional to the square of the denominator ratio $R$. It can be clearly seen from Figure 4 that the $\gamma$ value significantly influences $R$. $R$ increases sharply with the decrease of $\gamma$ value when coming into resonance. At a small $\gamma$ value, $R$ can be much larger than 1 at a broad laser energy range. In this circumstance, the RBM can be stronger than the G band.

The $\gamma$ value is determined by many factors, such as the phonon scattering, the tube−substrate interactions, defects, chirality, and diameter of SWCNTs.[47,48] For a perfect SWCNT without any perturbation, the $\gamma$ value is dominated by the inelastic scattering of phonons. The defects in the SWCNT could act as a scattering center for the carriers. Increase of the defects leads to the increase of the $\gamma$ value. Substrate−nanotube interaction may make the carrier relax from the SWNTs to the local energy levels in the substrates.[37] The additional relaxation paths could lead to shortening the lifetime of the excited carriers and broadening the $\gamma$ value. The SWCNTs suspended between silica spheres is grown without defects, as can be seen from the invisible D band. The suspended SWCNTs are also free of environmental effects. No defects and environmental effects make the $\gamma$ value of our sample smaller than the SWCNTs grown on a substrate with defects. After introducing defects into the nanotubes by functionalizing the SWCNTs with diazonium salts using previously published method,[49] the excited carriers could be scattered by the defects. The $\gamma$ increases in its value. In this case, we do not observe Raman signal with a large RBM/G band intensity ratio. The uniaxial strain may also affect the lifetime of the excited carriers. It is difficult for us to quantitatively determine the influence on $\gamma$ value. To solve this problem, isolated SWCNTs grown on trench-containing flat silicon wafer are used for control experiment. It can be seen

Single-Walled Carbon Nanotubes Grown on Silica

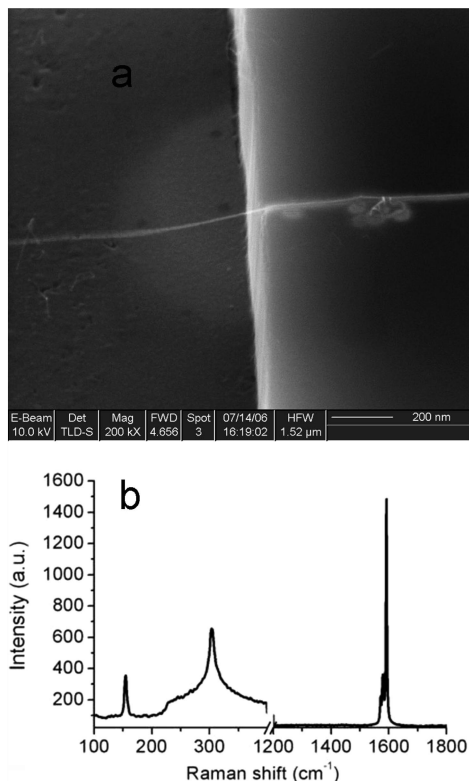*J. Phys. Chem. C, Vol. 113, No. 13, 2009* **5079**



**Figure 5.** SEM image (a) and the typical Raman spectrum (b) for an isolated SWCNT grown on a trench-containing silicon wafer.

from Figure 5 that the nanotube loosely suspends over the trench. Thus, there is no uniaxial strain imposed on these samples. For these suspended SWCNTs, although occasionally we can observe a strong RBM, the Raman signals show a G mode more intense than than that of the RBM in most cases. This fact indicates that it is the uniaxial strain other than the suspending of SWCNTs that mainly contributes to the intense RBM band. Then we can deduce that the uniaxial strain brings about a smaller $\gamma$ value, which leads to a larger RBM/G band intensity ratio.

## 4. Conclusion

Suspended SWCNTs grown on submicron silica spheres suffer from uniaxial strain. For these nanotubes, the lifetime of excited electronic states is longer than that of ordinary samples. The long lifetime of excited electronic states leads to the Raman signal with a large RBM/G band intensity ratio. The uniaxial strain does not shift the RBM and G band position for all the tubes. For semiconducting SWCNTs, the relative intensity of different modes of the G band changes significantly, while that of the metallic SWCNTs is maintained.

**Supporting Information Available:** Experimental details, more discussion about the strain induced in the samples and the discussion about the reason why Raman spectra were only from the suspended SWCNTs. This material is available free of charge via the Internet at http://pubs.acs.org.

## References and Notes

(1) Saito, R.; Dresselhaus, M. S.; Dresselhaus, G. *Physical Properties of Carbon Nanotubes*; World Scientific Publishing: Singapore, 1998.

(2) Dresselhaus, M. S.; Dresselhaus, G.; Jorio, A. *J. Phys. Chem. C* **2007**, *111*, 17887–17893.

(3) Araujo, P. T.; Doorn, S. K.; Kilina, S. T., S.; Einarsson, E.; Maruyama, S.; Chacham, H.; Pimenta, M. A.; Jorio, A. *Phys. Rev. Lett.* **2007**, *98*, 067401.

(4) Dresselhaus, M. S.; Dresselhaus, G.; Saito, R.; Jorio, A. *Phys. Rep.* **2005**, *409*, 47–99.

(5) Jorio, A.; Saito, R.; Hafner, J. H.; Lieber, C. M.; Hunter, M.; McClure, T.; Dresselhaus, G.; Dresselhaus, M. S. *Phys. Rev. Lett.* **2001**, *86*, 1118–1121.

(6) Rao, A. M.; Richter, E.; Bandow, S.; Chase, B.; Eklund, P. C.; Williams, K. W.; Fang, S.; Subbaswamy, K. R.; Menon, M.; Thess, A.; Smalley, R. E.; Dresselhaus, G.; Dresselhaus, M. S. *Science* **1997**, *275*, 187–191.

(7) Abdula, D.; Nguyen, K. T.; Shim, M. *J. Phys. Chem. C* **2007**, *111*, 17755–17760.

(8) Anderson, N.; Hartschuh, A.; Cronin, S.; Novotny, L. *J. Am. Chem. Soc.* **2005**, *127*, 2533–2537.

(9) Weisman, R. B.; Bachilo, S. M. *Nano Lett.* **2003**, *3*, 1235–1238.

(10) Milnera, M. J.; Kürti, M. H.; Kuzmany, H. *Phys. Rev. Lett.* **2000**, *84*, 1324–1327.

(11) Reich, S.; Thomsen, C.; Maultzsch, J. *Carbon Nanotubes: Basic Concepts and Physical Properties*; Wiley-VCH: Berlin, 2004.

(12) Kürti, J.; Zólyomi, V.; Kertesz, M.; Sun, G. *New J. Phys.* **2003**, *5* (125), 1.

(13) Bachilo, S. M.; Strano, M. S.; Kittrell, C. H., R. H.; Smalley, E., R.; Weisman, R. B. *Science* **2002**, *298*, 2361–2365.

(14) Meyer, J. C.; Paillet, M.; Michel, T.; More'ac, A.; Neumann, A.; Duesberg, G. S.; Roth, S.; Sauvajol, J.-L. *Phys. Rev. Lett.* **2005**, *95*, 217401.

(15) Paillet, M.; Langlois, S.; Sauvajol, J.-L.; Marty, L.; Iaia, A.; Naud, C.; Bouchiat, V.; Bonnot, A. M. *J. Phys. Chem. B* **2006**, *110*, 164–169.

(16) Paillet, M.; Michel, T.; Meyer, J. C.; Popov, V. N.; Henrard, L.; Roth, S.; Sauvajol, J.-L. *Phys. Rev. Lett.* **2006**, *96*, 257401.

(17) Kataura, H.; Kumazawa, Y.; Maniwa, Y.; Uemezu, I.; Suzuki, S.; Ohtsuka, Y.; Achiba, Y. *Synth. Met.* **1999**, *103*, 2555.

(18) Saito, R.; Takeya, T.; Kimura, T.; Dresselhaus, G.; Dresselhaus, M. S. *Phys. Rev. B* **1998**, *57*, 4145–4153.

(19) Jungen, A.; Popov, V. N.; Stampfer, C.; Durrer, L.; Stoll, S.; Hierold1, C. *Phys. Rev. B* **2007**, *75*, 041405.

(20) Popov, V. N.; Henrard, L.; Lambin, P. *Nano Lett.* **2004**, *4*, 1795–1799.

(21) Yu, Z.; Brus, L. E. *J. Phys. Chem. B* **2001**, *105*, 6831–6837.

(22) Cardona, M. *Top. Appl. Phys.* **1982**, *50*, 19–176.

(23) Martin, R. M.; Falicov, L. M. *Top. Appl. Phys.* **1983**, *8*, 79–145.

(24) Jiang, J.; Saito, R.; Grüneis, A.; Chou, S. G.; Samsonidze, G. G.; Jorio, A.; Dresselhaus, G.; Dresselhaus, M. S. *Phys. Rev. B* **2005**, *71*, 205420.

(25) Machón, M.; Reich, S.; Thomsen, C. *Phys. Rev. B* **2006**, *74*, 205423.

(26) Zhou, Z.; Dou, X.; Ci, L.; Song, L.; Liu, D.; Gao, Y.; Wang, J.; Liu, L.; Zhou, W.; Xie, S.; Wan, D. *J. Phys. Chem. B.* **2006**, *110*, 1206–1209.

(27) Fanchini, G.; Unalan, H. E.; Chhowalla, M. *Nano Lett.* **2007**, *7*, 1129–1133.

(28) Blackburn, J. L.; Engtrakul, C; M, T. J.; Dillon, A. C.; Heben, M. J. *J. Phys. Chem. B.* **2006**, *110*, 25551–25558.

(29) Ilie, A.; Bendall, J. S.; Roy, D.; Philp, E.; Green, M. L. H. *J. Phys. Chem. B.* **2006**, *110*, 13848–13857.

(30) Cronin, S. B.; Swan, A. K.; Unlu, M. S.; Goldberg, B. B.; Dresselhaus, M. S.; Tinkham1, M. *Phys. Rev. Lett.* **2004**, *93*, 167401.

(31) Cronin, S. B.; Swan, A. K.; Ünlü, M. S.; Goldberg, B. B.; Dresselhaus, M. S.; Tinkham, M. *Phys. Rev. B* **2005**, *72*, 035425.

(32) Duan, X.; Son, H.; Gao, B.; Zhang, J.; Wu, T.; Samsonidze, G. G.; Dresselhaus, M. S.; Liu, Z.; Kong, J. *Nano Lett.* **2007**, *7*, 2590–2595.

(33) Lee, S. W.; Jeong, G.-H.; Campbell, E. E. B. *Nano Lett.* **2007**, *7*, 2590–2595.

(34) Zhou, W.; Zhang, Y.; Li, X.; Li, Y. *J. Phys. Chem. B* **2005**, *109*, 6963–6967.

(35) Jin, Z.; Chu, H.; Wang, J.; Hong, J.; Tan, W.; Li, Y. *Nano Lett.* **2007**, *7*, 2073–2079.

(36) Kobayashi, Y.; Yamashita, T.; Ueno, Y.; Homma, Y.; Ogino, T. *Chem. Phys. Lett.* **2004**, *386*, 153–157.

(37) Xie, L.; Liu, C.; Zhang, J.; Zhang, Y.; Jiao, L.; Jiang, L.; Dai, L.; Liu, Z. *J. Am. Chem. Soc.* **2007**, *129* (41), 12382–12383.

(38) Jiang, J.; Ge., R. S.; Samsonidze, G.; Chou, S. G.; Jorio, A.; Dresselhaus, M. S.; Dresselhaus, G. *Phys. Rev. B* **2005**, *72*, 235408.

(39) Strano, M. S. *J. Am. Chem. Soc.* **2003**, *125*, 16148.

(40) Huang, M.; Wu, Y.; Chandra, B.; Yan, H.; Shan, Y.; Heinz, T. F.; Hone, J. *Phys. Rev. Lett.* **2008**, *100*, 136803.

(41) Maki, H.; Sato, T.; Ishibashi, K. *Nano Lett* **2007**, *7*, 890.

(42) Souza Filho, A. G.; Jiang, N. K., J.; Gruñeis, A.; Saito, R.; Cronin, S. B.; Mendes Filho, Ge, J.; Samsonidze, G.; Dresselhaus, G.; Dresselhaus, M. S. *Phys. Rev. Lett.* **2005**, *95*, 217403.

(43) Li, C.; Chou, T.-W. *Phys. Rev. B* **2005**, *71*, 235414.

(44) Huang, S. M.; Woodson, M.; Smalley, R.; Liu, J. *Nano Lett.* **2004**, *4*, 1025.

(45) Hertel, T.; Walkup, R. E.; Avouris, P. *Phys. Rev. B* **1998**, *58*, 13870.

(46) Son, H. B.; Samsonidze, G.; Kong, J.; Zhang, Y.; Duan, X. J.; Zhang, J.; Liu, Z. F.; Dresselhaus, M. S. *Appl. Phys. Lett.* **2007**, *90*, 253113.

(47) Jorio, A.; Fantini, C.; Dantas, M. S. S.; Pimenta, M. A.; Filho, A. G. S.; Samsonidze, G. G.; Brar, W.; Dresselhaus, G.; Dresselhaus, M. S.; Swan, A. K.; nlü, M. S. U.; Goldberg, B. B.; Saito, R. *Phys. Rev B* **2002**, *66*, 15411.

(48) Park, J. S.; Oyama, Y.; Saito.; Izumida, W.; Jiang, J.; Sato, K.; Fantini, C.; Jorio, A.; Dresselhaus, G.; Dresselhaus., M. S. *Phys. Rev. B* **2006**, *74*, 165414.

(49) Strano, M. S.; Dyke, C. A.; Usrey, M. L.; Barone, P. W.; Allen, M. J.; Shan, H.; Kittrell, C.; Hauge, R. H.; Tour, J. M.; Smalley, R. E. *Science* **2003**, *301*, 1519.